coatings

MDPI

Communication

Experimental Investigation on the Droplet Stability of Superhydrophobic Mesh

Dong Song *, Xin Liu, Xiang Wang, Xiaoxu Du and Haibao Hu

School of Marine Science and Technology, Northwestern Polytechnical University, 127 Youyi Xilu, Xi'an 710072, China
* Correspondence: songdong1226@nwpu.edu.cn

Abstract: Superhydrophobic surfaces could repel water due to the capillary force associated with surface roughness, which has a large range of applications, such as underwater drag reduction, heat transfer enhancement, oil/water separation, and so on. However, the engineering applications of superhydrophobic surfaces rely on the stability of the superhydrophobic surfaces. In this study, a hydrophilic metal mesh was modified to be superhydrophobic. The resulting superhydrophobic mesh was designed as a bowl capable of holding water without leaking and as a boat floating on top of water without sinking. The stability of an impacting droplet on a superhydrophobic mesh was investigated using both experiments and theoretical analysis. It was demonstrated that the capillary force is able to prevent water from passing through the mesh and maintain the stability of the air–water interface under dynamic pressure. Furthermore, a theoretical model was developed to diagnose the stability of the air–water interface on the superhydrophobic mesh when in contact with water, and the results are consistent with the experimental findings. The results of this work can be utilized to design robust superhydrophobic meshes and advance the field of droplet manipulation.

Keywords: superhydrophobic; mesh; contact time; air–water interface stability

check for updates

Citation: Song, D.; Liu, X.; Wang, X.; Du, X.; Hu, H. Experimental Investigation on the Droplet Stability of Superhydrophobic Mesh. *Coatings* **2023**, *13*, 756. https://doi.org/10.3390/coatings13040756

Academic Editor: Ludmila B. Boinovich

Received: 11 March 2023
Revised: 7 April 2023
Accepted: 8 April 2023
Published: 10 April 2023

Copyright: © 2023 by the authors. Licensee MDPI, Basel, Switzerland. This article is an open access article distributed under the terms and conditions of the Creative Commons Attribution (CC BY) license (https://creativecommons.org/licenses/by/4.0/).

1. Introduction

Inspired by the lotus effect, a superhydrophobic surface, composed of microstructures and low surface energy materials, is able to trap a thin air layer within the microstructures [1–3]. The air layer is trapped between solid micro-sized surface roughness and fluids, which is stable [4,5]. Due to the air–water interface on the superhydrophobic surface that contacts with water, the superhydrophobic surface can be widely applied in a series of engineering applications, such as underwater drag reduction [6–13], heat transfer enhancement [14–17], droplet manipulation [18–21], de-icing techniques for outdoor facilities [17,22], microfluidics [23,24], oil–water separation [25–28], and so on. When a mesh is modified to be superhydrophobic, with the surface roughness decreasing to a micron scale, the role of the capillary force plays a more important role in the macro phenomenon of water on it. For example, when a large droplet impacts a superhydrophobic mesh array, monodisperse droplets will be generated, which is useful in microfluidic engineering, materials science, and drug production. A superhydrophobic mesh could be an efficient approach to separate oil from water [29–31]. It could be used to enhance the water collection rate from the atmosphere and fog via a superhydrophobic mesh [32].

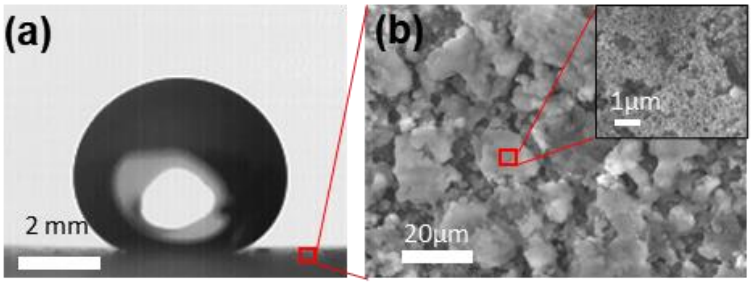
The stability of the air–water interface on the superhydrophobic surface is one of the most concerning factors for engineering applications. When air–water lies on the micron surface structures, it is supported by the Laplace pressure, which increases with the decrease in the size of the surface micro-structures [33,34]. As a result, superhydrophobic surfaces with nano-sized structures have been proposed to enhance the robustness of superhydrophobicity [35]. What is more, inspired by the "Salvinia effect", hydrophilic spots have also been introduced into a superhydrophobic substrate to enhance the air

stability on the superhydrophobic surfaces [36,37]. When a mesh, with holes of ~100 μm, is coated with a superhydrophobic coating made of nano-sized roughness, the dual-sized structures can make the mesh superhydrophobic, where a novel interfacial phenomenon appears [38–40]. When a droplet impacts a superhydrophobic wire, it will be divided into halves [41]. When a droplet impacts a superhydrophobic mesh, a portion of the water droplet will pass through the mesh with submillimeter pores during impact [40]. According to the lattice Boltzmann simulation, the inertial effect dominates the spread stage of droplet impact [38]. The dual-sized structures can make the mesh superhydrophobic; however, the relatively large holes on the mesh make the air–water interface very weak. It should be noted that theoretical analysis associated with experimental investigations on the stability of the air–water interface on superhydrophobic meshes is still lacking due to the complex interaction between the capillary and inertia force. In this work, a superhydrophobic mesh is fabricated, and the stability is investigated experimentally.

2. Experimental Setup

2.1. Modification of the Wettability of the Mesh

The stainless-steel mesh without treatment was hydrophilic. To make it superhydrophobic, a lab-made superhydrophobic coating was prepared in advance. The superhydrophobic coating was a mixture of hydrophobic SiO_2 nanoparticles (Aerosil RX300) with a diameter of 100 nm and a binder of methylphenyl silicone resin (SR355S, Momentive Performance Materials), both of which were pre-mixed in acetone [42,43]. The solution was mixed with an ultrasonic stirrer for 10 min. Then, the coating was spray-coated on the stainless-steel mesh and dried in the air for 2 h. As shown in Figure 1, the superhydrophobic coating shows a very large contact angle at ~165°.



(c)

Sample	Diameter (*d*,mm)	Spacing (*w*, mm)
bare	/	/
1#	0.3	1.7
2#	0.15	0.9
3#	0.1	0.6

Figure 1. (**a**) Contact angle of a droplet on the surface coated with the superhydrophobic coating. (**b**) SEM image of the superhydrophobic coating. (**c**) Size of the tested mesh, where *d* and *w* are the diameter of the mesh fiber and the spacing of the fibers of the mesh, respectively.

The stability of the superhydrophobic mesh was robust. As shown in Figure 2a,b, the superhydrophobic mesh was shaped into a bowl; it could take water as high as 10 mm with a volume of ~25 mL. What is more, the superhydrophobic bowl of mesh could take water from a container dynamically without leaking, as shown in Video S1.mp4 of the supporting information. The superhydrophobic bowl could even float on top of the water. As shown in Figure 2c and Video S2.mp4 of the supporting information, the superhydrophobic mesh did not sink on top of water, even with a load as high as 25 g on it.

2.2. Experimental Setup for Tests of an Impacting Droplet on a Superhydrophobic Mesh

The stability of the air–water interface of the superhydrophobic mesh was evaluated via the impacting test using a high-speed camera, as shown in Figure 3. A droplet was released from a needle with a volume of 9 μL. The impacting velocity was changed by varying the releasing height. A piece of mesh, 15 mm wide and 50 mm long, was fixed right below the needle. A high-speed camera (Revealer, M120, Hefei, China) was used to capture the impacting process at speed of 1000 fps.

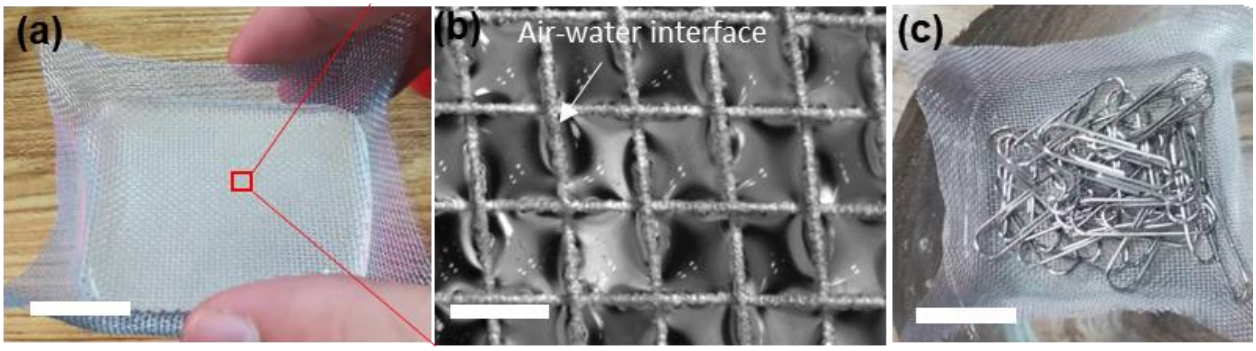


Figure 2. (**a**) Superhydrophobic bowl that could carry water. (**b**) Air–water interface at the bottom of the superhydrophobic bowl. (**c**) A superhydrophobic mesh of stainless steel that could carry loads floating on top of water. Scale bars in (**a**–**c**) are 10 mm, 1 mm, and 10 mm, respectively.

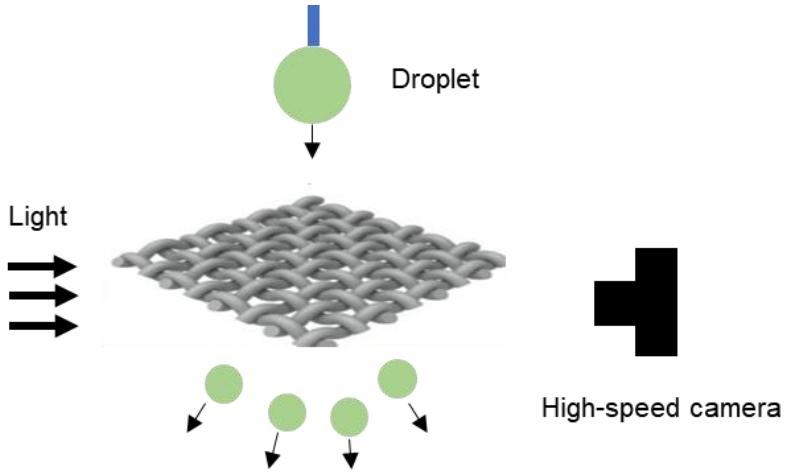


Figure 3. Schematic of the experimental setup to test the stability of water on mesh.

3. Results and Discussion

3.1. Impacting Process of a Droplet on Different Substrates

When a water droplet impacts a superhydrophobic surface, it rebounds off the surface in a short time due to the low surface energy between the water and superhydrophobic substrate, as shown in Figure 4a. Previous experiments indicated that the contact time of the impacting droplet on the superhydrophobic surface, t_c, is independent of the dimensionless Weber number, $We = \rho V^2 R/\gamma$, where ρ, V, R, and γ are the water density, impacting velocity, the radius of the droplet, and the surface tension of water in the air, respectively [44,45]. More specifically, the contact time is proportional to an inertial–capillary timescale $\tau = \sqrt{\rho R^3/\gamma}$ [44]. For the droplet in our experiments, $\tau = 5.5$ ms. A previous study has shown, both theoretically and experimentally, that the relationship between the real contact time and the inertial–capillary timescale of a droplet is $t_c/\tau = \pi/2.2$, which is independent of the size and fluid property of the droplet [44]. This equation can predict the contact time precisely if the droplet maintains one unit after the impact. In our experiments, droplets with an impacting speed in a range between 0.4 m/s and 1.0 m/s were tested, and t_c/τ was between 2.1 and 2.3, which agrees well with the prediction on the bare superhydrophobic surface.

When a droplet impacts the hydrophilic mesh, as shown in Figure 4b, the droplet passes through the mesh and is split by the fiber during the early stage of the impacting process. Due to the hydrophilicity of the mesh substrate, the water sticks to the hydrophilic mesh after passing through the mesh, hanging on it without falling.

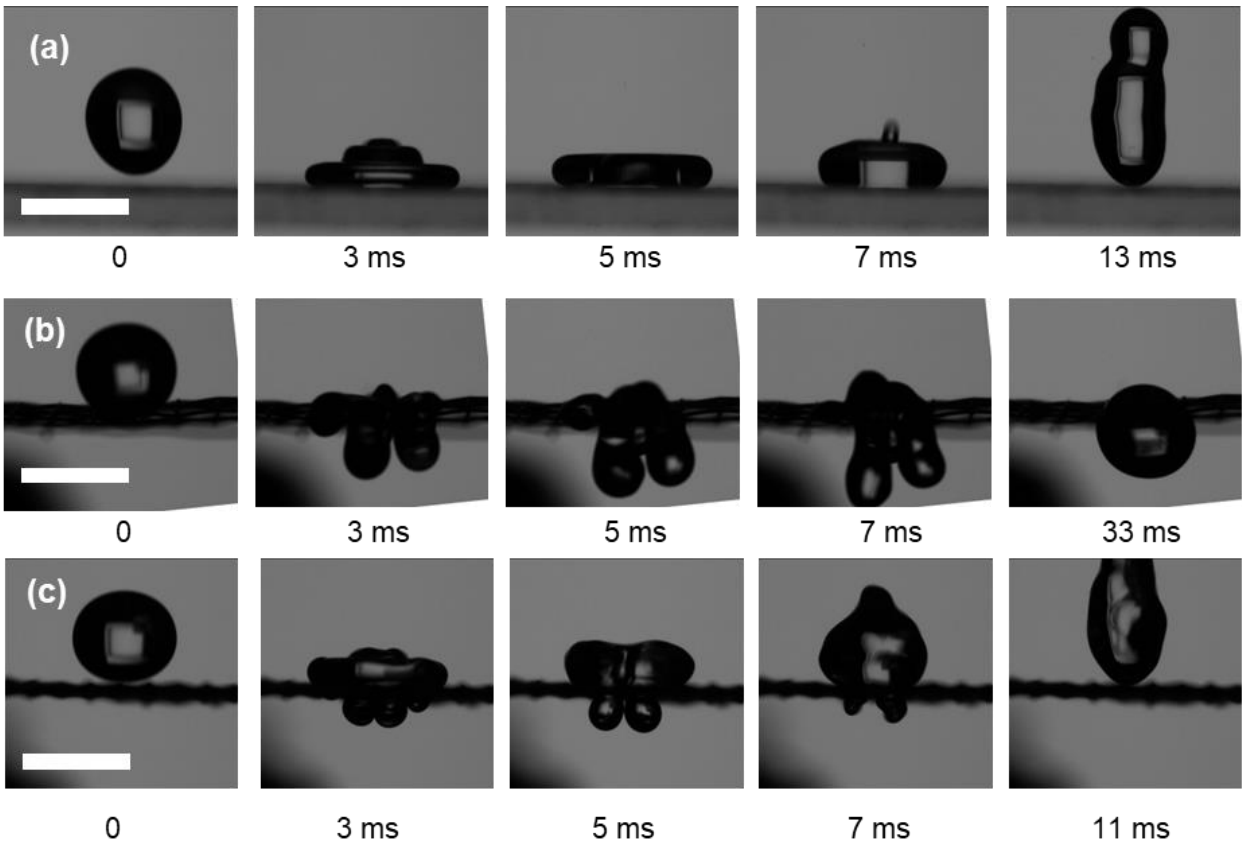


Figure 4. Impacting process of a droplet on different substrates. (**a**) Superhydrophobic substrate. (**b**) Hydrophilic mesh. (**c**) Superhydrophobic mesh. The mesh in (**b**,**c**) is NO. 2#. The impact speed of the droplet is 0.6 m/s. Scale bars are 3 mm.

When a droplet impacts the superhydrophobic mesh, as shown in Figure 4c, the droplet is still able to rebound off the substrate if the impacting speed is slower than 0.6 m/s on 2# mesh. However, in the early stage of the impacting process, as shown in the third image of Figure 4c, part of the droplet passes through the gap between the mesh fibers and is stopped by the surface tension. Eventually, the droplet rebounds off the superhydrophobic mesh, and the contact time of the droplet on the superhydrophobic mesh was 11 ms, which is much smaller than the value predicted by ref. [44] and 15% shorter than the one on a bare superhydrophobic substrate. The reduced contact time of droplets on the superhydrophobic mesh comes from the fluid passing through the hollow mesh and contracting during the rebounding period [46].

3.2. Stability of Impacting Water on Superhydrophobic Mesh

When a droplet rests on the superhydrophobic mesh, the air–water interface on the gap is maintained by Laplace pressure, as shown in Figure 5a. The Laplace pressure is caused by the curvature of the air–water interface, $\Delta P = 2\frac{\gamma}{r}$, where r is the radius of the interface curvature. For the air–water interface between the gap of the mesh fibers, $r \geq 0.5w$. As a result, the Laplace pressure is $\Delta P \leq 4\gamma/w$. The maximum of the Laplace pressure, $\Delta P = 4\gamma/w$, increases as the size of the gap of the mesh decreases. When a droplet impacts on a superhydrophobic mesh, as shown in Figure 5b, the dynamic pressure, $0.5\rho U^2$, transfers to static pressure, P, during the slowing period of the early stage. To make the air–water stable, the following condition should be maintained:

$$\Delta P = \frac{4\gamma}{w} \gg 0.5\rho V^2 \quad (1)$$

When the speed of the impacting droplet is relatively small, the Laplace pressure is high enough to maintain the air–water interface, as shown in Figure 4c. However, as the droplet speed overcomes a critical value,

$$V \leq \sqrt{8\gamma/w\rho} \tag{2}$$

the droplet is split into several parts and part of the droplet passes through the mesh. As shown in Figure 6, at a relatively high impacting speed, part of the droplet passes through the mesh and is divided into several tiny droplets. The rest of the droplet rebounds off the superhydrophobic mesh upward.

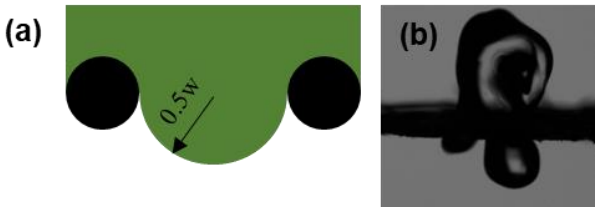


Figure 5. (**a**) Schematic diagram of the Laplace pressure that holds the water above the superhydrophobic mesh. (**b**) Instantaneous image of an impacting droplet on the superhydrophobic mesh (NO. 1#).

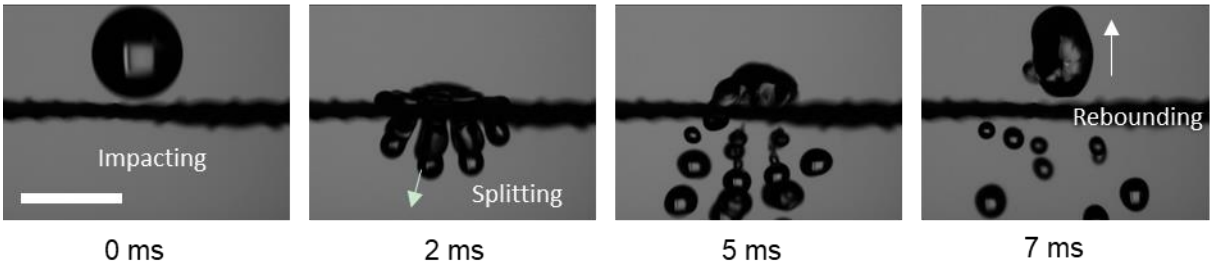


Figure 6. Breaking process of the droplet on the superhydrophobic mesh. The impacting velocity is 0.99 m/s. The mesh is NO. 2#. Scale bar is 3 mm.

The critical velocity for the droplet collapsing on the superhydrophobic mesh changes as a function of the width of the mesh gap, as shown in Figure 7. Equation (2) agrees well with experimental results, which shows that an impacting droplet is easier to collapse and is divided by the mesh as the size of the mesh gap increases.

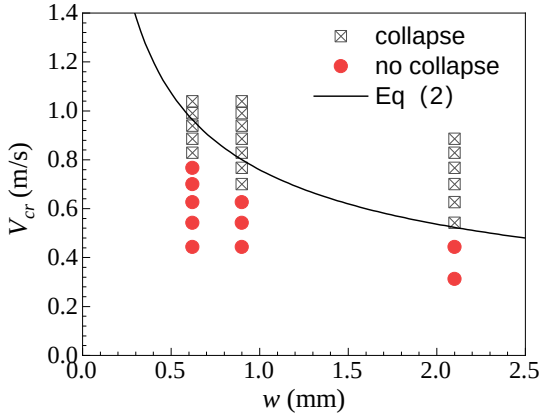


Figure 7. Critical velocity for the droplet collapsing on the superhydrophobic mesh changes as a function of the width of the mesh gap (w).

The size of the gap of the mesh affects the splitting behavior. As shown in Figure 8, where only one droplet is divided by the superhydrophobic mesh, the size of the first divided droplet increases as the size of the gap increases. Since the mesh with a larger gap holds a smaller Laplace pressure, it is easier for the droplet splitting behavior to happen on the superhydrophobic mesh with a larger gap.

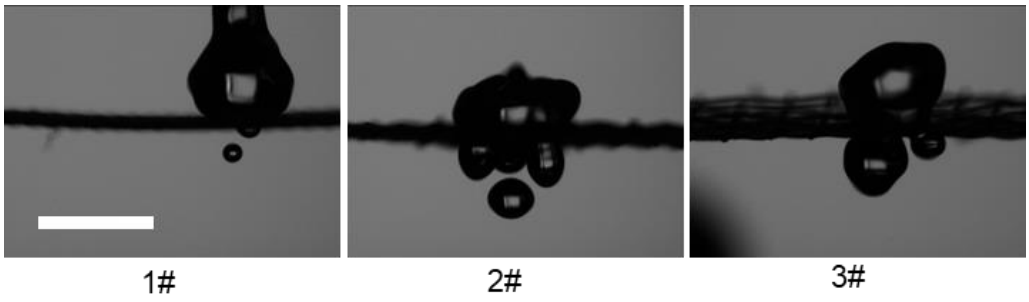


Figure 8. Effect of mesh size on the droplet cutting process. Scale bar is 3 mm.

3.3. Contact Time of Droplet on the Superhydrophobic Mesh

Figure 9 shows the contact time of a droplet on different substrates. As a droplet impacts a bare solid superhydrophobic surface, the contact time is independent of the impacting speed, i.e., $t_c = 2.2\sqrt{\rho R^3/\gamma}$ [44]. However, the contact time of the droplet on the superhydrophobic mesh is not constant and decreases as the impacting speed increases on the superhydrophobic mesh. On No. 2 of the superhydrophobic mesh, the normalized contact time of the droplet is only 54% of the one on the bare superhydrophobic substrate at *We* = 17.

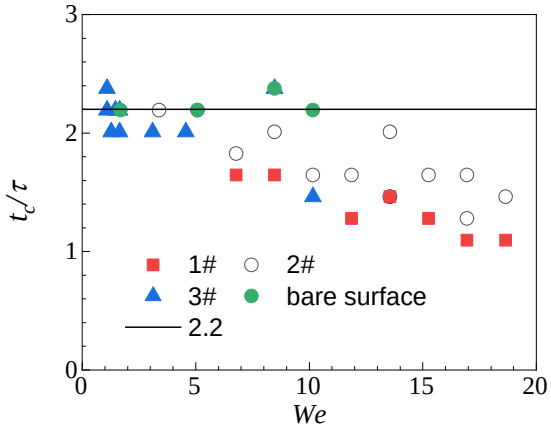


Figure 9. Normalized contact time of a droplet on the superhydrophobic mesh.

The impacting velocity affects the dividing process of the impacting droplet on the superhydrophobic mesh significantly. As shown in Figure 10, as the impacting speed increases, the number of divided tiny droplets that pass through the superhydrophobic mesh increases. For example, when the impacting speed is 0.44 m/s on 2# superhydrophobic mesh, where the width of the mesh gap is 0.9 mm, only one tiny droplet (with a diameter of ~ 0.6 mm and a volume of ~0.11 μL) passes through the mesh. However, over 10 tiny droplets are divided from the droplet and pass through the mesh as the impacting velocity increases to 1.00 m/s, and the volume of the rest of the droplet is much smaller than the original one. As shown in the last image of Figure 10, the diameter of the droplet that rebounds off the superhydrophobic mesh is R'~1 mm, where $t' = 2.2\sqrt{\rho R'^3/\gamma} \approx 8$ ms and $t'/t \sim 61\%$, which agrees well with the real contact time of the droplet.

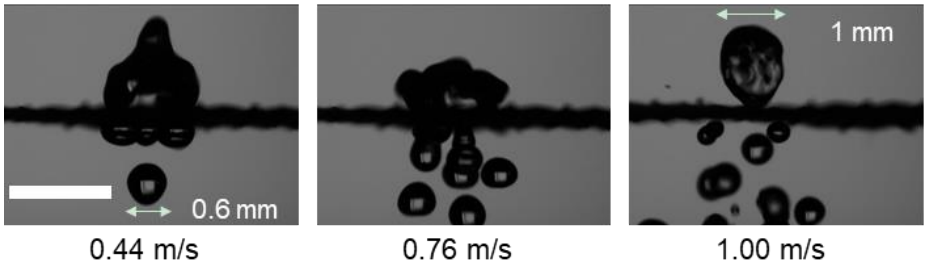


Figure 10. Effect of impacting velocity on the droplet cutting process. The mesh is NO. 2. Scale bar is 3 mm.

4. Conclusions

The impacting process of a droplet on a superhydrophobic mesh was investigated. The Laplace pressure is able to maintain the air–water interface on the superhydrophobic mesh, which can serve as a bowl to carry water and a boat floating on top of the water with loads. The stability of the air–water interface was investigated based on the balance between the Laplace pressure and the dynamic pressure, which agrees well with experiments. When the dynamic pressure is higher than the Laplace pressure, part of the impacting droplet is divided into tiny droplets by the superhydrophobic mesh, which passes through the mesh, and the rest of the droplet rebounds off the surface in a shorter time compared to the one on a regular superhydrophobic surface. Due to the reduced volume of the droplet, the contact time of the droplet on the superhydrophobic mesh is reduced at the same time. The findings from this research can be applied to develop durable superhydrophobic meshes and make significant strides in the area of droplet control.

Supplementary Materials: The following supporting information can be downloaded at: https://www.mdpi.com/article/10.3390/coatings13040756/s1, Video S1, Video S2.

Author Contributions: Conceptualization, D.S.; methodology, X.L.; validation, X.W., X.D. and H.H.; writing—original draft preparation, D.S. and X.L.; supervision, D.S. All authors have read and agreed to the published version of the manuscript.

Funding: This research was funded by the National Science Foundation of China (grant numbers: 12002282 and 51879218), the Fundamental Research Funds for the Central Universities (grant number: 3102020HHZY030006).

Institutional Review Board Statement: Not applicable.

Informed Consent Statement: Not applicable.

Data Availability Statement: Not applicable.

Conflicts of Interest: The authors declare no conflict of interest.

References

1. Neinhuis, C.; Barthlott, W. Characterization and distribution of water-repellent, self-cleaning plant surfaces. *Ann. Bot.* **1997**, *79*, 667–677. [CrossRef]
2. Cassie, A.; Baxter, S. Wettability of porous surfaces. *Trans. Faraday Soc.* **1944**, *40*, 546–551. [CrossRef]
3. Erdene-Ochir, O.; Chun, D.-M. Robust Superhydrophobic Surface on Polypropylene with Thick Hydrophobic Silica Nanoparticle-Coated Films Prepared by Facile Compression Molding. *Energies* **2021**, *14*, 3155. [CrossRef]
4. Emami, B.; Vahedi Tafreshi, H.; Gad-el-Hak, M.; Tepper, G.C. Predicting shape and stability of air–water interface on superhydrophobic surfaces comprised of pores with arbitrary shapes and depths. *Appl. Phys. Lett.* **2012**, *100*, 013104. [CrossRef]
5. Song, D.; Song, B.; Hu, H.; Du, X.; Du, P.; Choi, C.-H.; Rothstein, J.P. Effect of a surface tension gradient on the slip flow along a superhydrophobic air-water interface. *Phys. Rev. Fluids* **2018**, *3*, 033303. [CrossRef]
6. Rothstein, J.P. Slip on Superhydrophobic Surfaces. *Annu. Rev. Fluid Mech.* **2010**, *42*, 89–109. [CrossRef]
7. Srinivasan, S.; Kleingartner, J.A.; Gilbert, J.B.; Cohen, R.E.; Milne, A.J.B.; McKinley, G.H. Sustainable Drag Reduction in Turbulent Taylor-Couette Flows by Depositing Sprayable Superhydrophobic Surfaces. *Phys. Rev. Lett.* **2015**, *114*, 014501. [CrossRef]
8. Aljallis, E.; Sarshar, M.A.; Datla, R.; Sikka, V.; Jones, A.; Choi, C.-H. Experimental study of skin friction drag reduction on superhydrophobic flat plates in high Reynolds number boundary layer flow. *Phys. Fluids* **2013**, *25*, 025103. [CrossRef]

9. Ou, J.; Perot, B.; Rothstein, J.P. Laminar drag reduction in microchannels using ultrahydrophobic surfaces. *Phys. Fluids* **2004**, *16*, 4635–4643. [CrossRef]
10. Srinivasan, S.; Choi, W.; Park, K.C.; Chhatre, S.S.; Cohen, R.E.; McKinley, G.H. Drag reduction for viscous laminar flow on spray-coated non-wetting surfaces. *Soft Matter* **2013**, *9*, 5691–5702. [CrossRef]
11. Choi, C.H.; Ulmanella, U.; Kim, J.; Ho, C.M.; Kim, C.J. Effective slip and friction reduction in nanograted superhydrophobic microchannels. *Phys. Fluids* **2006**, *18*, 087105. [CrossRef]
12. Song, D.; Daniello, R.J.; Rothstein, J.P. Drag reduction using superhydrophobic sanded Teflon surfaces. *Exp. Fluids* **2014**, *55*, 1783. [CrossRef]
13. Hoai Thanh, N.; Chang, K.; Lee, S.-W.; Ryu, J.; Kim, M. Numerical Prediction of Turbulent Drag Reduction with Different Solid Fractions and Distribution Shapes over Superhydrophobic Surfaces. *Energies* **2022**, *15*, 6645.
14. Yang, Q.; Sun, P.Z.; Fumagalli, L.; Stebunov, Y.V.; Haigh, S.J.; Zhou, Z.W.; Grigorieva, I.V.; Wang, F.C.; Geim, A.K. Capillary condensation under atomic-scale confinement. *Nature* **2020**, *588*, 250–253. [CrossRef]
15. Jiang, M.; Wang, Y.; Liu, F.; Du, H.; Li, Y.; Zhang, H.; To, S.; Wang, S.; Pan, C.; Yu, J. Inhibiting the Leidenfrost effect above 1,000° C for sustained thermal cooling. *Nature* **2022**, *601*, 568–572. [CrossRef]
16. Cui, J.; Cui, Y. Effects of Surface Wettability and Roughness on the Heat Transfer Performance of Fluid Flowing through Microchannels. *Energies* **2015**, *8*, 5704–5724. [CrossRef]
17. Okulov, V.; Kabardin, I.; Mukhin, D.; Stepanov, K.; Okulova, N. Physical De-Icing Techniques for Wind Turbine Blades. *Energies* **2021**, *14*, 6750. [CrossRef]
18. Yarin, A.L. Drop impact dynamics: Splashing, spreading, receding, bouncing . . . . *Annu. Rev. Fluid Mech.* **2006**, *38*, 159–192. [CrossRef]
19. Zhang, X.; Zhu, Z.; Zhang, C.; Yang, C. Reduced contact time of a droplet impacting on a moving superhydrophobic surface. *Appl. Phys. Lett.* **2020**, *117*, 151602. [CrossRef]
20. Song, D.; Bhushan, B. Optimization of bioinspired triangular patterns for water condensation and transport. *Philos. Trans. R. Soc. A Math. Phys. Eng. Sci.* **2019**, *377*, 20190127. [CrossRef]
21. Song, D.; Bhushan, B. Bioinspired triangular patterns for water collection from fog. *Philos. Trans. R. Soc. A Math. Phys. Eng. Sci.* **2019**, *377*, 20190128. [CrossRef] [PubMed]
22. Song, D.; Jiang, Y.; Chou, T.; Asawa, K.; Choi, C.-H. Spontaneous Deicing on Cold Surfaces. *Langmuir* **2020**, *36*, 11245–11254. [CrossRef]
23. Xing, S.; Jiang, J.; Pan, T. Interfacial microfluidic transport on micropatterned superhydrophobic textile. *Lab Chip* **2013**, *13*, 1937–1947. [CrossRef]
24. Vinogradova, O.I.; Dubov, A.L. Superhydrophobic textures for microfluidics. *Mendeleev Commun.* **2012**, *22*, 229–236. [CrossRef]
25. Lei, S.; Fang, X.; Wang, F.; Xue, M.; Ou, J.; Li, C.; Li, W. A facile route to fabricate superhydrophobic Cu_2O surface for efficient oil–water separation. *Coatings* **2019**, *9*, 659. [CrossRef]
26. Chen, Y.; Yang, S.; Zhang, Q.; Zhang, D.; Yang, C.; Wang, Z.; Wang, R.; Song, R.; Wang, W.; Zhao, Y. Effects of Surface Microstructures on Superhydrophobic Properties and Oil-Water Separation Efficiency. *Coatings* **2019**, *9*, 69. [CrossRef]
27. Wang, C.-F.; Tsai, Y.-J.; Kuo, S.-W.; Lee, K.-J.; Hu, C.-C.; Lai, J.-Y. Toward superhydrophobic/superoleophilic materials for separation of oil/water mixtures and water-in-oil emulsions using phase inversion methods. *Coatings* **2018**, *8*, 396. [CrossRef]
28. Xue, Z.; Cao, Y.; Liu, N.; Feng, L.; Jiang, L. Special wettable materials for oil/water separation. *J. Mater. Chem. A* **2014**, *2*, 2445–2460. [CrossRef]
29. Ren, G.; Song, Y.; Li, X.; Zhou, Y.; Zhang, Z.; Zhu, X. A superhydrophobic copper mesh as an advanced platform for oil-water separation. *Appl. Surf. Sci.* **2018**, *428*, 520–525. [CrossRef]
30. Ammann, S.; Ammann, A.; Ravotti, R.; Fischer, L.J.; Stamatiou, A.; Worlitschek, J. Effective Separation of a Water in Oil Emulsion from a Direct Contact Latent Heat Storage System. *Energies* **2018**, *11*, 2264. [CrossRef]
31. Yuan, J.; Cui, C.; Qi, B.; Wei, J.; Qaisrani, M.A. Experimental Investigation of Copper Mesh Substrate with Selective Wettability to Separate Oil/Water Mixture. *Energies* **2019**, *12*, 4564. [CrossRef]
32. Kang, J.H.; Lee, J.-W.; Kim, J.Y.; Moon, J.W.; Jang, H.S.; Jung, S.Y. Effect of mesh wettability modification on atmospheric and industrial fog harvesting. *Front. Phys.* **2021**, *9*, 680641. [CrossRef]
33. Song, D.; Song, B.; Hu, H.; Du, X.; Ma, Z. Contact angle and impinging process of droplets on partially grooved hydrophobic surfaces. *Appl. Therm. Eng.* **2015**, *85*, 356–364. [CrossRef]
34. Liu, Y.; Tan, X.; Li, X.; Xiao, T.; Jiang, L.; Nie, S.; Song, J.; Chen, X. Eco-Friendly Fabrication of Transparent Superhydrophobic Coating with Excellent Mechanical Robustness, Chemical Stability, and Long-Term Outdoor Durability. *Langmuir* **2022**, *38*, 12881–12893. [CrossRef]
35. Wen, G.; Guo, Z.; Liu, W. Biomimetic polymeric superhydrophobic surfaces and nanostructures: From fabrication to applications. *Nanoscale* **2017**, *9*, 3338–3366. [CrossRef]
36. Bing, W.; Wang, H.; Tian, L.; Zhao, J.; Jin, H.; Du, W.; Ren, L. Small structure, large effect: Functional surfaces inspired by salvinia leaves. *Small Struct.* **2021**, *2*, 2100079. [CrossRef]
37. Babu, D.J.; Mail, M.; Barthlott, W.; Schneider, J.J. Superhydrophobic vertically aligned carbon nanotubes for biomimetic air retention under water (Salvinia effect). *Adv. Mater. Interfaces* **2017**, *4*, 1700273. [CrossRef]

38. Wang, G.; Gao, J.; Luo, K.H. Droplet impacting a superhydrophobic mesh array: Effect of liquid properties. *Phys. Rev. Fluids* **2020**, *5*, 123605. [CrossRef]
39. Mehrizi, A.A.; Lin, S.; Sun, L.; Wang, Y.; Chen, L. Penetration and ligament formation of viscoelastic droplets impacting on the superhydrophobic mesh. *Sci. Rep.* **2022**, *12*, 11920. [CrossRef]
40. Ryu, S.; Sen, P.; Nam, Y.; Lee, C. Water penetration through a superhydrophobic mesh during a drop impact. *Phys. Rev. Lett.* **2017**, *118*, 014501. [CrossRef]
41. Song, D.; Xu, C.; Song, B.; Pan, G.; Hu, H.; Choi, C.-H. Splitting an Impacting Droplet by a Superhydrophobic Wire. *Coatings* **2022**, *12*, 1866. [CrossRef]
42. Song, D.; Bhushan, B. Enhancement of water collection and transport in bioinspired triangular patterns from combined fog and condensation. *J. Colloid Interface Sci.* **2019**, *557*, 528–536. [CrossRef] [PubMed]
43. Song, D.; Bhushan, B. Water condensation and transport on bioinspired triangular patterns with heterogeneous wettability at a low temperature. *Philos. Trans. R. Soc. A* **2018**, *377*, 20180335. [CrossRef] [PubMed]
44. Richard, D.; Clanet, C.; Quéré, D. Contact time of a bouncing drop. *Nature* **2002**, *417*, 811. [CrossRef]
45. Bird, J.C.; Dhiman, R.; Kwon, H.-M.; Varanasi, K.K. Reducing the contact time of a bouncing drop. *Nature* **2013**, *503*, 385–388. [CrossRef]
46. Liu, Y.; Moevius, L.; Xu, X.; Qian, T.; Yeomans, J.M.; Wang, Z. Pancake bouncing on superhydrophobic surfaces. *Nat. Phys.* **2014**, *10*, 515–519. [CrossRef]

Disclaimer/Publisher's Note: The statements, opinions and data contained in all publications are solely those of the individual author(s) and contributor(s) and not of MDPI and/or the editor(s). MDPI and/or the editor(s) disclaim responsibility for any injury to people or property resulting from any ideas, methods, instructions or products referred to in the content.